Heliyon 7 (2021) e06369

Contents lists available at ScienceDirect

Heliyon

journal homepage: www.cell.com/heliyon

Research article

# CFD and statistical approach to optimize the average air velocity and air volume fraction in an inert-particles spouted-bed reactor (IPSBR) system

A. Mohammad [a], A.A.H.I. Mourad [a,c], A.H. Al-Marzouqi [a], M.H. El-Naas [d,*], B. Van der Bruggen [e], M. Al-Marzouqi [a], F. Alnaimat [b], M. Suleiman [f], M. Al Musharfy [f]

[a] Department of Chemical and Petroleum Engineering, UAE University, Al Ain, United Arab Emirates
[b] Department of Mechanical Engineering, UAE University, Al Ain, United Arab Emirates
[c] Academic Support Department, Abu Dhabi Polytechnic, Institute of Applied Technology, Abu Dhabi, United Arab Emirates
[d] Gas Processing Center, College of Engineering, Qatar University, Doha, Qatar
[e] Department of Chemical Engineering, KU Leuven, Leuven, Belgium
[f] ADNOC Refining Research Center, Abu Dhabi, United Arab Emirates

ARTICLE INFO

*Keywords:*
Computational fluid dynamics
Eulerian model
Gas–liquid reactor
Regression analysis
Optimization
Response surface methodology

ABSTRACT

Inert-particles spouted bed reactor (IPSBR) is characterized by intense mixing generated by the circular motion of the inert particles. The operating parameters play an important role in the performance of the IPSBR system, and therefore, parameter optimization is critical for the design and scale-up of this gas–liquid contact system. Computational fluid dynamics (CFD) provides detailed modeling of the system hydrodynamics, enabling the determination of the operating conditions that optimize the performance of this contact system. The present work optimizes the main IPSBR operating parameters, which include a feed-gas velocity in the range 0.5–1.5 m/s, orifice diameter in the range 0.001–0.005 m, gas head in the range 0.15–0.35 m, mixing-particle diameter in the range 0.009–0.0225 m, and mixing-particle to reactor volume fraction in the range 2.0–10.0 vol % (which represents 0.01–0.1 kg of mixing particles loading). The effects of these parameters on the average air velocity and average air volume fraction in the upper, middle, and conical regions of the reactor were studied. The specific distance for each region has been measured from the orifice point to be 50 mm for the conical region, 350 mm for the middle region and 550 mm for the upper rejoin. The selected factors were optimized to obtain the minimum air velocity distribution (maximum gas residence time) and the maximum air volume fraction (maximum interfacial area concentration) because these conditions will increase the gas holdup, the gas–liquid contact area, and the mass transfer coefficient among phases. Response surface methodology (RSM) was used to determine the optimum operating conditions. The regression analysis showed an excellent fit of the experimental data to a second-order polynomial model. The interaction between the process variables was evaluated using the obtained three-dimensional surface plots. The analysis revealed that under the optimized parameters of a feed-gas velocity of 1.5 m/s, orifice diameter of 0.001 m, gas head of 0.164 m, mixing-particle diameter of 0.0225 m, and mixing-particle loading of 0.02 kg, the minimum average air velocity and highest air volume fraction were observed throughout the reactor.

## 1. Introduction

Spouted beds have many advantages and applications compared with other moving beds, due to their ability to handle granular particles with a wide range of size distribution. Inert particles spouted bed reactor (IPSBR) is a special case of a spouted bed, where a gas jet is injected at the bottom of a conical vessel containing liquid and coarse inert particles. The system was developed and tested by El-Naas et al. [1, 2] for the reaction of $CO_2$ with ammoniated brine. The interfacial area, mass and heat transfer were found to be enhanced by the addition of mixing particles [3]. Ibrahim et al. [4] examined the reaction of $CO_2$ with electric arc furnace bag house dust (EAF BHD) in the presence of desalination reject brine using a similar IPSBR. They reported significant impact of the inert particle mixing on carbon dioxide uptake, achieving an optimum update of 0.2 g $CO_2$/g BHD at 24°C temperature and 1 atm pressure. A previous study simulated the hydrodynamics of this reactor (IPSBR)

* Corresponding author.
*E-mail address:* muftah@qu.edu.qa (M.H. El-Naas).

https://doi.org/10.1016/j.heliyon.2021.e06369
Received 17 October 2020; Received in revised form 3 December 2020; Accepted 22 February 2021
2405-8440/© 2021 Published by Elsevier Ltd. This is an open access article under the CC BY-NC-ND license (http://creativecommons.org/licenses/by-nc-nd/4.0/).

using a transient two-dimensional (2-D) axisymmetric model via computational fluid dynamics (CFD) with coupled Eulerian and discrete phase model (CFD-DPM) [5]. Turbulence was simulated by the standard k-ϵ mixture model, and DPM was applied to consider the effect of mixing particles. The results showed that the stagnant zones near the walls were reduced by the addition of the mixing particles. The conical shape of this contact system increased the gas residence time and holdup. Hence, the overall reaction efficiency was improved. Moreover, the model results were verified by comparison with the results from a laboratory-scale IPSBR. The model data were found to be in good quantitative agreement with the experimental results.

CFD simulation was implemented by Zhao et al. [6] to study the performance of particle flow patterns of 2 dimensional spouted bed that has a rectangular shape with width of 152 mm and depth of 15 mm. It was noticed that low Reynolds number k–ε turbulence model improved the prediction of spout shape and particle flow patterns. It was also observed that the particles displayed the greatest drag and acceleration values near the spout entrance. Moreover, the drag forces continuously reduce as particles moved upward in the spout. Eulerian two-fluid model was implemented by Jiang et al. [7] to study the effect of operating pressure on the flow behaviors of the spouted bed. By increasing the pressure, more reduction in the minimum spouting velocity was observed. The mixing behaviors of binary particle mixtures with equal diameter (4 mm) and different density in a spouted bed by three-dimensional CFD had been investigated [8]. It was confirmed that the quality of mixing increased by increasing the gas velocity and reduced by increasing the density of particles. Ren et al. [9] developed a 3-D CFD model to simulate gas-solid turbulent flow in a cylindrical spouted bed with a conical base. Hosseini et al. [10]; studied the influence of different operating parameters on the pressure drop in a conical spouted bed with binary particle mixtures. Results showed that, increasing the bed cone angle resulted in an increase in the maximum pressure drop and minimum spouting velocity.

A comprehensive parametric sensitivity analysis is important in view of improving the design, scale-up, and operation of moving bed reactors. Optimizing any process requires a good understanding of the complex relationships among the influential factors Response surface methodology (RSM) is a powerful statistical technique that can be used to optimize and model a wide range of engineering systems [11]. Santos et al. [12] used the RSM to investigate the effect of mixture composition and static bed height on the air flow rate and pressure drop of a spouted bed with binary mixtures. CFD (Eulerian Granular Multiphase) simulations were implemented and verified with results from the literature. It was concluded that the axial and radial profiles of volume fraction illustrated a coherent behavior for the largest particles when compared with the literature data. Pashaei et al. [13] used Central Composite Design (CCD) which is a method within RSM to optimize $CO_2$ absorption in a bubble column for the piperazine–$H_2O$–$CO_2$ system. Their results indicated that, under the optimized conditions, a maximum $CO_2$ removal efficiency of 97.9% and a $CO_2$ loading of 0.258 mol/mol were achieved. Nuchitprasittichai et al. [14] developed a simulation-optimization framework that combines a process simulator with RSM. They investigated the effects of the absorber and stripper column heights, the operating conditions, and the concentration of amine solvents on the cost of $CO_2$ removal by the amine-based absorption process. They concluded that 48 wt% diglycolamine, which led to 96% $CO_2$ elimination, was the lowest-cost process because of its high $CO_2$ absorption capability and low energy consumption. Gholamzadehdevin et al. [15] investigated the hydrodynamics of an activated-sludge bubble column by CFD. They implemented design of experiment and full-factorial design to determine the effect of the superficial gas velocity, tracer injection position, and the sparger type on the mixing time. Their results illustrated that the superficial gas velocity was the variable that most strongly influenced system performance. In addition, they found that the hydrodynamic performance was improved by modifications to the gas sparger. Liang et al. [16] optimized the production of β-alanine in a bubble column reactor with a 200 mL working volume by RSM in combination with a 23-factor central composite experimental design. The optimum operating conditions were obtained by a quadratic polynomial predictive model. They concluded that a 40.6% increase in β-alanine production was achieved with a cell loading of 16.50 gww/200 mL, substrate concentration of 1.29% (v/v), and air flowrate of 86.56 L/h. Aghbolaghy et al. [17] combined CFD and RSM to simulate and optimize a continuous stirred-tank reactor for enzymatic production of hydrogen peroxide. A good distribution of particles inside the reactor was observed. They reported that the optimal operating conditions were a pure water flowrate of 20.57 L/min, glucose molar rate of 0.64 gmol/min, and impeller speed of 375 rpm. They also observed a good agreement between experimental and CFD–RSM results. Prabhu et al. [18] optimized the hydrodynamic parameters of a counter-flow inverse fluidized-bed reactor. They used RSM and an artificial neural network to study the effect of bed volume, superficial liquid velocity, and superficial gas velocity on the percentage bed expansion, average pressure drop, liquid holdup, gas holdup, and the solid holdup.

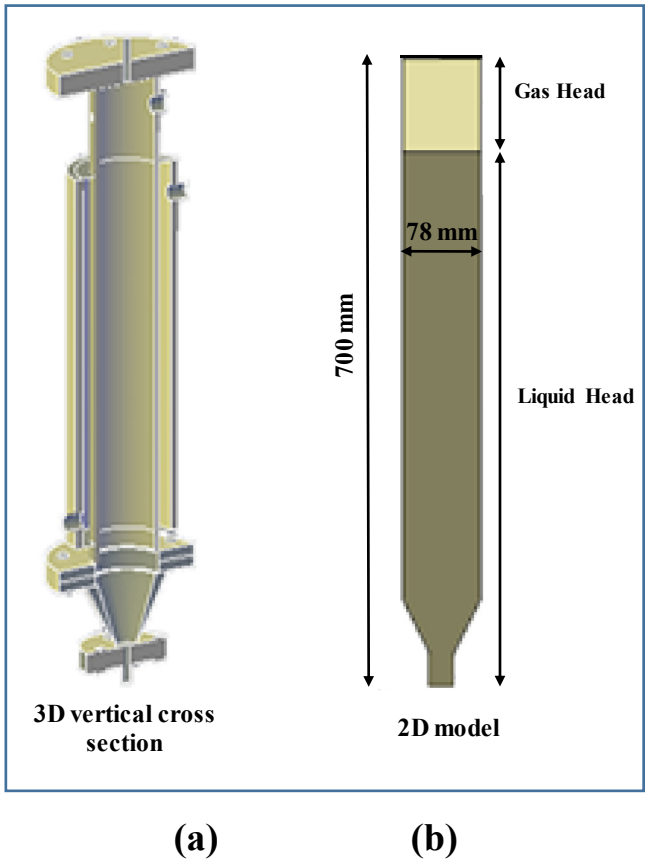


**Figure 1.** IPSBR system with 3D vertical cross section and simulated 2D model with major dimensions and gas/liquid heads.

RSM has also been reported to be more effective in revealing the factors that most strongly contribute to the regression coefficient and in identifying insignificant quadratic terms. The main objective of the present work is to optimize the hydrodynamic parameters of the IPSBR [1, 2, 5]. CFD simulation has been combined with RSM to study the effect of the feed-gas velocity, orifice diameter, gas head, diameter of mixing particles, and the mixing particles loading on the average air velocity distribution and gas volume fraction in the IPSBR.

## 2. CFD simulation

### 2.1. Simulated geometry and particles

The IPSBR [5] has an internal diameter of 78 mm and an overall height of 700 mm. It was operated in a semi-batch mode, where the liquid was exposed to a continuous flow of gas through an orifice with a specific diameter. The gas head is the distance filled by air above the liquid surface before starting the air flow from the bottom through the liquid head and mixing particles as shown in Figure 1. The mixing inert particles, which are added to the reactor content, have a sphericity value of one.

The computational grid and mesh structure of the contact system were generated using the GAMBIT 2.4.6 software described elsewhere [4]. A structure with 2-D geometry was established in semi-batch mode and then imported into ANSYS Fluent 18.0 to simulate the flow of gas into the contact system [4]. The contact system was initially filled with a specific amount of water. The internal diameter and height of the contact system were 0.078 m and 0.850 m, respectively, and the total working volume of water was 3000 ml. The water level increased after the gas started to flow; therefore, the air space was kept at the top of the reactor [4].

The mesh independency was studied in previous work [4] by investigating the air velocity distribution at a specific height over the gas inlet. Seven mesh sizes from 0.0022 m to 0.0016 m were examined. A grid size of 0.0020 m was selected, which corresponds to a cell count of 32,871, because it provided a difference of only 2.6% from the finest tested mesh. Hence, the 0.0020 m mesh was applied in the current 2-D CFD study.

### 2.2. Governing equations for the CFD simulations

Eulerian method is useful for solving multiphase and turbulent flow. Liquid and gas phases are considered to be two separate phases interacting with each other in a computational domain. The volume fraction of the gas and liquid phases were solved by a separate volume fraction equation in each computational cell. In addition, momentum and continuity equations are solved for each phase. The realizable k–ε model had been employed to consider the turbulence effects of the flow of gas through water [19].

The details of the governing equations used to describe the flow in the contact system are shown as follows [5, 20, 21]:

Continuity Equation

$$\frac{\partial}{\partial t}(\alpha_k \rho_k) + \nabla.(\alpha_k \rho_k \vec{v}_m) = \sum_{p=1}^{n}(\dot{m}_{pk} - \dot{m}_{kp}) + S_k \tag{1}$$

where $\vec{v}_m$ is the mixture velocity, $\dot{m}_{pk}$ characterizes the mass transfer from the p$^{th}$ to k$^{th}$ phase, $\dot{m}_{kp}$ characterizes the mass transfer from the k$^{th}$ to p$^{th}$ phase, which is equal to 0, and $S_k$ is the source/sink term, which is equal to zero since there is no chemical reaction or phase change in the simulation process. Eq. (1) can be written as:

$$\frac{\partial}{\partial t}(\alpha_k \rho_k) + \nabla.\left(\alpha_k \rho_k \vec{v}_m\right) = \sum_{p=1}^{n} \dot{m}_{pk} \tag{2}$$

Momentum Equation

$$\frac{\partial}{\partial t}\left(\alpha_k \rho_m \vec{v}_m\right) + \nabla.\left(\alpha_k \rho_k \vec{v}_m \vec{v}_m\right) = -\alpha_k \nabla P + \alpha_k \rho_k \vec{g} + \nabla.\bar{\bar{\tau}}_k + \sum_{p=1}^{n}\left(\vec{R}_{pk} + \dot{m}_{pk}\vec{v}_k\right) + \alpha_k \rho_k\left(\vec{F}_k + \vec{F}_{lift,k} + \vec{F}_{\text{virtual mass},k}\right) \tag{3}$$

where $\bar{\bar{\tau}}_k$ is the $k$th phase stress–strain tensor, whose components are given as

$$\tau_{k,ij} = \alpha_k \mu_k\left(\frac{\partial v_{k,j}}{\partial x_j} + \frac{\partial v_{k,j}}{\partial x_i}\right) - \frac{2}{3}\alpha_k \mu_k \delta_{ij}\frac{\partial v_{k,i}}{\partial x_i} \tag{4}$$

The inter-phase exchange forces are expressed as

$$\vec{R}_{pk} = K_{pk}\left(\vec{v}_q - \vec{v}_k\right) \tag{5}$$

where $K_{pk}$ is the momentum exchange coefficient between the $p$th and $k$th phases.

#### 2.2.1. Mixing particles

Mixing particles were shown to provide greater interfacial area between the gas and liquid and thereby enhance gas reactivity. In addition, the gas was reported to be perfectly distributed into the reactor and hence improved the mass and heat transfer between phases [4]. The inert particles used in the contact system previously [1] were made of polymethyl methacrylate with an average particle diameter of 0.013 m, density of 1020 kg/m$^3$, surface area of 4.92 cm$^2$/particle, and sphericity of 1.0; these particles were also used in the present study. In the discrete phase model, the trajectory of the particles was tracked using the Newtonian equation of motion [5, 22]:

$$\frac{\partial v_p}{\partial t} = f_D(v - v_p) + \frac{g(\rho_p - \rho)}{\rho_p} + f \tag{6}$$

where $f_D$ is the resistance impacting on a unit-mass particle and $f_D(v - v_p)$ represents the air resistance impacting on the particle

$$f_D = \frac{3\,\mu\, C_D Re}{4\rho_p d_p^2} \tag{7}$$

where $v$ is the fluid velocity, $v_p$ is the particle velocity, $\mu$ is the fluid molecular viscosity, $\rho$ is the fluid density, $\rho_p$ is the particle density, and $d_p$ is the particle diameter. $Re$ is the relative Reynolds number, which is defined as

$$R_e = \frac{\rho d_p |v_p - v|}{\mu} \tag{8}$$

The drag coefficient, $C_D$, is defined as

$$C_D = a_1 + \frac{a_2}{R_e} + \frac{a_3}{R_e^2} \tag{9}$$

where $a_1$ $a_2$, and $a_3$ are constants that can be applied for smooth spherical particles over different ranges of $Re$. The a's are defined as following [23]:

$$a_1, a_2, a_3 = \begin{cases} 0,\ 24,\ 0 & 0 < R_e < 0.1 \\ 3.690,\ 22.73,\ 0.0903 & 0.1 < R_e < 1 \\ 1.222,\ 29.1667,\ -3.8889 & 1 < R_e < 10 \\ 0.6167,\ 46.50,\ -116.67 & 10 < R_e < 100 \\ 0.3644,\ 98.33,\ -2778 & 100 < R_e < 1000 \\ 0.357,\ 148.62,\ -47500 & 1000 < R_e < 5000 \\ 0.46,\ -490.546,\ 578700 & 5000 < R_e < 10000 \\ 0.5191,\ -1662.5,\ 5416700 & R_e \geq 10000 \end{cases} \tag{10}$$

### 2.3. Numerical methodology and simulation conditions

The numerical solution was obtained using the ANSYS FLUENT 18.0 software. Hydrodynamic flow behavior was investigated using the Eulerian multiphase model. The numerical analysis program dealt with isothermal, unsteady, incompressible, two-phase flow, and constant gas phase properties. Atmospheric pressure was imposed at the top of the column. Water was considered the primary phase, whereas air was

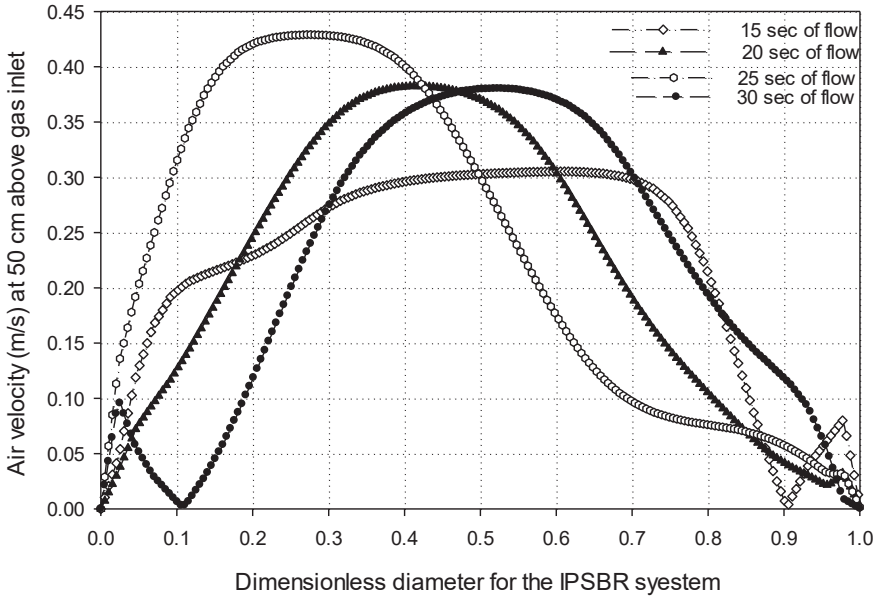


**Figure 2.** Quasi-steady state investigation for semi-batch mode at different flow times (15–30 s) for gas velocity of 1 m/s and without mixing particles [5].

considered the secondary phase. Bubbles of equal diameter in the range 0.001–0.005 m for each run were formed through a spherical orifice at the bottom of the reactor. Coalescence and breakage properties were neglected. The total volume fraction of the two phases was considered as one. In addition, a no-slip boundary condition was assumed at the solid wall. The simulations were conducted under transient and gravitational acceleration conditions. The standard $k$–$\varepsilon$ model was applied. A phase-coupled simple scheme with volume fractions was implemented to solve the momentum and pressure equations. The least-squares cell-based method [5, 24] was used to calculate the gradient. Momentum and turbulence equations were solved by a first-order upwind scheme [5, 25, 26, 27]. The under-relaxation factors for pressure and momentum were set as 0.7. The column was partially filled with water; then, at time $t = 0.0$ s, air was injected through the orifice at a velocity of 1 m/s. The finite volume method was used to solve the numerical model. For solution initialization, a hybrid initialization method was used. A step size of 0.00001 was selected for all runs, and 20 iterations per time step were selected for each run to increase both the efficiency and accuracy of the simulation results. For each time step the convergence criterion of $10^{-3}$ was used as the convergence indicator. According to the results of the quasi-steady-state test reported before [5], the time at which accurate results can be recorded is 20 s or longer. The time-averaged profile for the

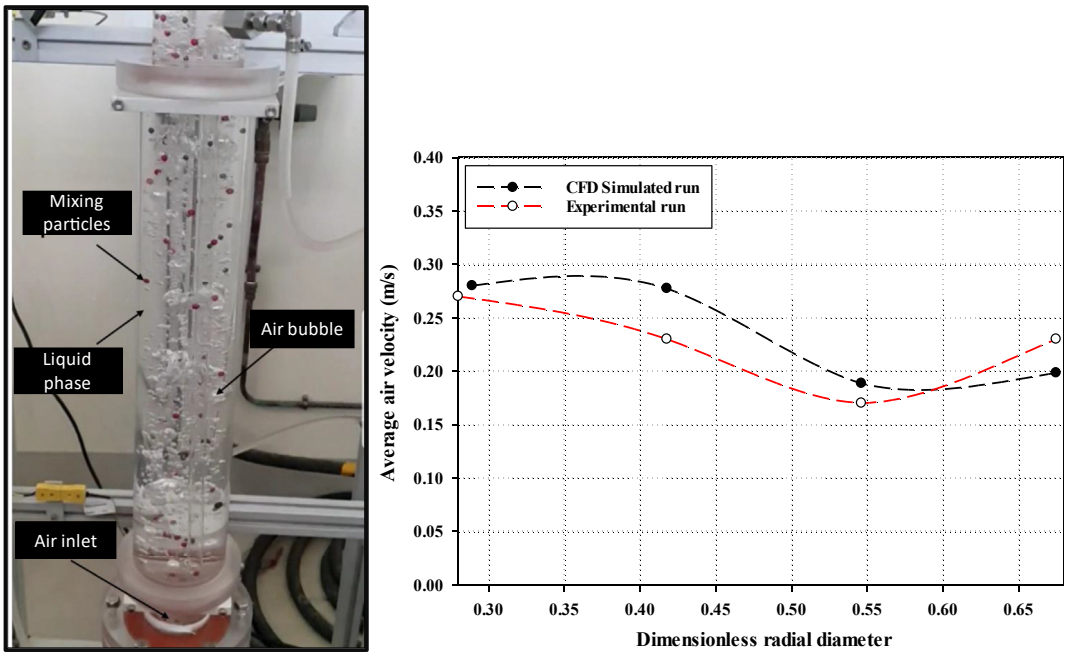


**Figure 3.** (a) A laboratory-scale IPSBR with inert mixing particles and (b) Experimental and simulation results for average air velocity at certain point (50 mm from orifice diameter) at the same operating conditions (mixing particles diameter of 0.005 m, orifice diameter of 0.002 m, gas velocity of 0.5 m/s, gas head of 0.25 m and mixing particles loading of 0.02 kg [5].

**Table 1.** Levels of parameters and their variation limits for CCD runs.

| | Factors | | | | |
|---|---|---|---|---|---|
| Levels | Feed gas velocity | Orifice diameter | Gas head | Diameter of mixing particles | Mixing particle loading |
| Units | m/s | m | M | m | kg |
| Tag | V | OD | GH | DM | FM |
| Symbol | $X_1$ | $X_2$ | $X_3$ | $X_4$ | $X_5$ |
| Level -α | 0.5 | 0.001 | 0.15 | 0.009 | 0.02 |
| Level -1 | 0.75 | 0.002 | 0.2 | 0.0045 | 0.04 |
| Level 0 | 1 | 0.003 | 0.25 | 0.0135 | 0.06 |
| Level +1 | 1.25 | 0.004 | 0.3 | 0.018 | 0.08 |
| Level +α | 1.5 | 0.005 | 0.35 | 0.0225 | 0.1 |

transient state has been previously calculated at 25 and 30 s time intervals (averaged data over 5 s of flow was chosen) [5]. In this work, the time-averaged profile for the transient state has been selected to be over 60–65 s time interval to insure more stability of the quasi steady state. The standard error deviation was in the range of (0.00429–0.00961).

### 2.4. The quasi-steady state conditions

A quasi-steady state test has been conducted to identify the correct time at which the results of bubble column could be recorded. As shown in Figure 2, the optimum time at which the results should be recorded is around 20 s where the air velocity distribution achieved the quasi-steady state [5]. However, to insure a safe margin of flow time value in the presented CFD work, considering all the turbulence effect of the mixing particles and different gas feed velocities, a 60 s of flow is considered in all runs.

### 2.5. CFD validation

A laboratory-scale IPSBR with a geometry consistent with the studied geometry was used to validate the Eulerian model reported in a previous work [7] as shown in Figure 3 (a). The reactor was filled with spherical particles with a diameter of 0.005 m. A gas orifice with an inner diameter of 0.002 m is installed at the bottom of the system. Figure 3 (b) presents the experimental and simulation results at 50 mm from orifice point. the same operating conditions (mixing particles diameter of 0.005 m, orifice diameter of 0.002 m, gas velocity of 0.5 m/s, gas head of 0.25 m and mixing particles loading of 0.02 kg) was considered for the experimental and simulated runs. The observed change in velocities are in good agreement with the CFD results with a deviation of only 5–10 %.

## 3. Numerical optimization (RSM) design

The effects of the independent process parameters (i.e., feed-gas flowrate, orifice diameter, gas head, diameter of the mixing particles, and mixing particles loading) on dependent process responses (i.e., the average air velocity and average air volume fraction) were investigated by full-factorial CCD design using Minitab 19.0 software. A total of 32 runs with five levels of each factor were chosen. Table 1 lists these parameters (factors) along with the selected levels for each. Conditions for each run were inserted to ANSYS Fluent and then all data obtained from the simulation (responses) were analyzed using RSM. It is worth mentioning that the mixing particles, which were used in the validation experiments, had a size of 0.005 m. For the numerical optimization, the following mixing particles diameters were considered: 0.009, 0.0045, 0.0135, 0.018, and 0.0225. Therefore, the validated mixing particles size, 0.005 m, was within the statistical tested range of the mixing particles diameter.

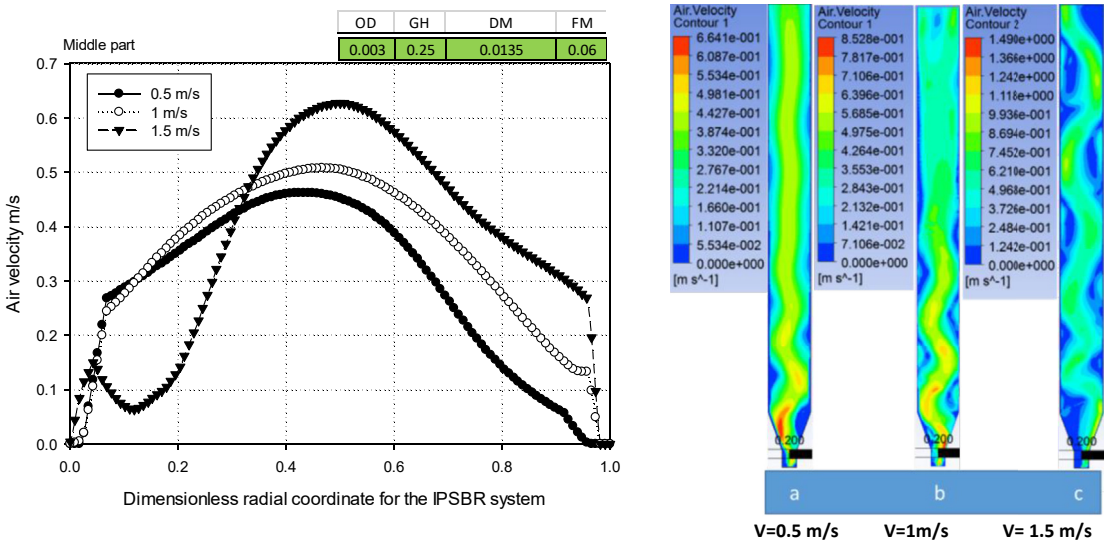


(a) (b)

**Figure 4.** (a) The effect of feed gas velocity on the horizontal profile of the time-averaged gas velocity at constant orifice diameter of 0.003 m, gas head of 0.25 m, mixing particles diameter of 0.0135 m and mixing particles loading of 0.06 kg at the middle region and (b) Eulerian model contours over the three regions for the effect of feed gas velocity on the air velocity distribution at the same fixed conditions.

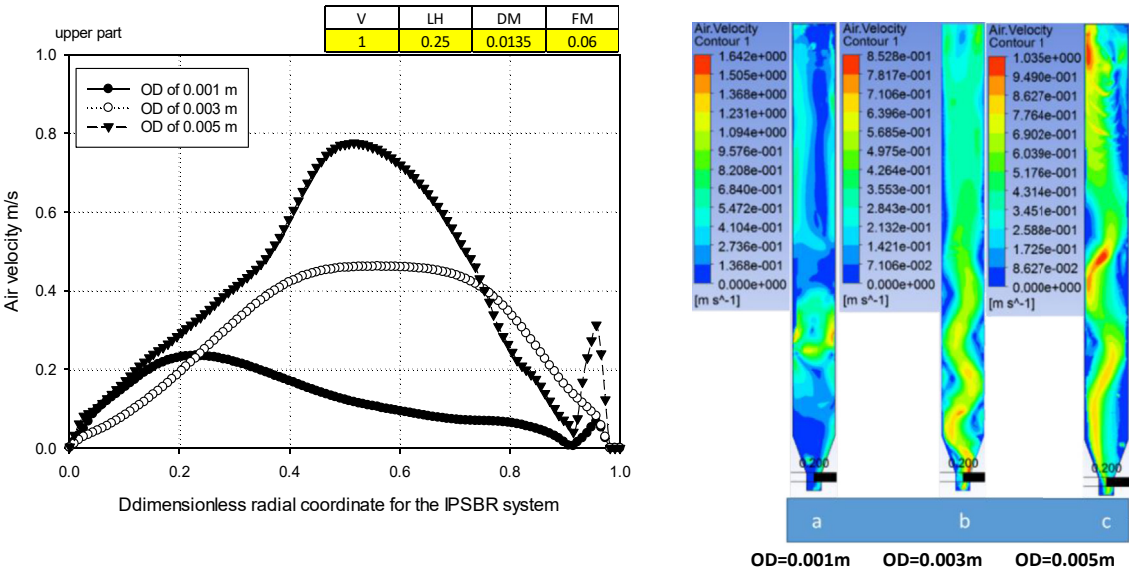


(a) (b)

**Figure 5.** (a) Effect of orifice diameter on the averaged on horizontal profile of the time-averaged gas velocity at constant feed gas velocity of 1 m/s, gas head of 0.25 m, mixing particles diameter of 0.0135 m and mixing particles loading of 0.06 kg at the upper region and (b) Eulerian model contours over the three regions for the effect of orifice diameter on the air velocity distribution at the same fixed conditions.

RSM is a statistical and mathematical technique commonly applied to engineering modeling and optimization design [28, 29, 30]. The relationship between input factors and obtained responses can be quantified by RSM [31]. CCD is an extensively used form of RSM and is effective for constructing a quadratic model. The following second-order polynomial response equation was used to correlate the response variable (average air velocity and average air volume fraction) to the independent variables [32]:

$$Y = \beta_{\circ} + \sum_{i=1} \beta_i x_i + \sum_{i=1} \beta_{ii} x_i^2 + \sum_{i=1} \sum_{j=i+1} \beta_{ij} x_i x_j \quad (11)$$

where $Y$ is defined as the response function, $\beta_o$ is the constant coefficient, $\beta_i$ determines the influence of the variable $i$ in the response (linear effect coefficient), $\beta_{ii}$ parameters define the shape of the curve (squared effect coefficient), $x_i$ is the variable $i$ coded value, $x_j$ is the variable $j$ coded value, and $\beta_{ij}$ is the interaction effect coefficient. The coded values were calculated according to the following equation:

$$x_i = \frac{X_i - X_o}{\delta x} \quad (12)$$

where $X_0$ is value of $X_i$ at the center of the domain and δx is the step change.

## 4. Results and discussion

### 4.1. Effect of independent parameters on the air velocity distribution

a) *Effect of feed-gas velocity on air velocity distribution*

Figure 4(a) illustrates the effect of the feed-gas velocity on the air velocity distribution at the middle region of the contact system versus the dimensionless radial coordinate. The results were observed at a constant orifice diameter of 0.003 m, gas head of 0.25 m, mixing-particle diameter of 0.0135 m, and mixing-particle loading of 0.06 kg. The asymmetry behavior of the velocity profile as shown in the figure can be explained by the presence of the mixing particles, which causes turbulent circular motion and deviates the velocity profile from symmetry. In addition, for the middle region and specifically at the selected cross sectional area, as the feed gas velocity increased from 0.5-1.5 m/s, the time-averaged air velocity increased by 26% (from 0.278 to 0.350 m/s). However, as an overall trend, the average air velocity over the whole contact system (total area not one specific cross sectional area) decreased by 84% when the feed gas velocity was increased from 0.5 to 1.5 m/s. This is consistence with the findings related to the change in average gas velocity inside a bubble column reactor. It has been reported in the literature that increasing the mass flow rate of the feed gas and accordingly the superficial gas velocity will lead to an increase in the total gas hold up and, consequently, the average gas velocity inside the contact system will decrease [33, 34]. This result confirms the effectiveness of the reactor, because it can operate at a high feed-gas flowrate and hence improve the overall performance of the system by treating large amounts of gas effluents. The conical design and the presence of mixing particles improve the air and liquid flow contacts inside the reactor, thus increasing the gas residence time. Figure 4(b) shows the air velocity contours for the Eulerian model at different feed-gas flowrates at the same fixed conditions.

b) *Effect of orifice diameter on air velocity distribution*

The changes in air velocity at the conical, middle, and upper regions were evaluated for three different orifice diameters (0.001, 0.003, and 0.005 m). The results were extracted for a constant feed-gas velocity of 1 m/s, gas head of 0.25 m, mixing-particle diameter of 0.0135 m, and mixing-particle loading of 0.06 kg, the results for the upper region is presented in Figure 5 (a). According to the simulated data, it was found that the change in air velocity increased further at 0.003 and 0.005 mm compared to that at 0.001 mm, consistent with the increase in the cross-sectional contact area between the gas and liquid. In addition, the trend in the middle part is similar to that in the upper part: the minimum velocity (0.11 m/s) was observed at the orifice diameter of 0.001 mm and started to increase until reaching a peak value of 0.8 m/s at diameters of 0.003 and 0.005 mm. Bubble size is determined by the size of the orifice diameter, where a smaller orifice diameter enables the formation of

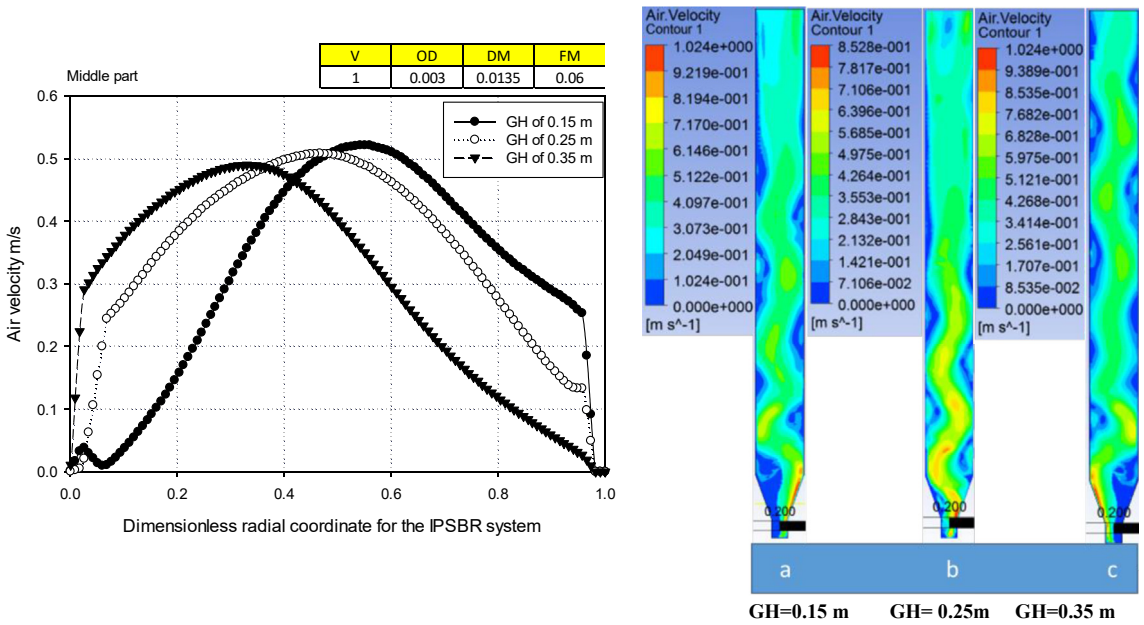


**Figure 6.** (a) Effect of gas head on the horizontal profile of the time-averaged gas velocity at constant feed gas velocity of 1 m/s, orifice diameter of 0.003 m, mixing particles diameter of 0.0135 m and mixing particles loading of 0.06 kg at the middle region and (b) Eulerian model contours over the three regions for the effect of gas head on the air velocity distribution at the same fixed conditions.

smaller bubbles and, hence, a lower velocity is recorded [35]. The gas residence time and holdup have been observed to increase with decreasing bubble size [36]. Figure 5 (b) depicts the contours of the air velocity for 0.001, 0.003, and 0.005 mm orifice diameters.

c) *Effect of gas head on air velocity*

The effect of gas head on air velocity distribution was studied at constant feed-gas velocity of 1 m/s, orifice diameter of 0.003 m, mixing-particle diameter of 0.0135 m, and mixing-particle loading of 0.06 kg at the middle region. As expected, a uniform trend for gas velocity was not observed at the conical region because the selected cross-sectional area is smaller than the cross-sectional areas in the middle and upper regions, which causes a substantial disturbance in the air velocity.

The mixing particles also play an important role in causing a high coalescence among bubbles, especially in this region, which is considered the injection zone for the mixing particles [37]. As the gas bubbles move from the conical region toward the middle and upper regions, their

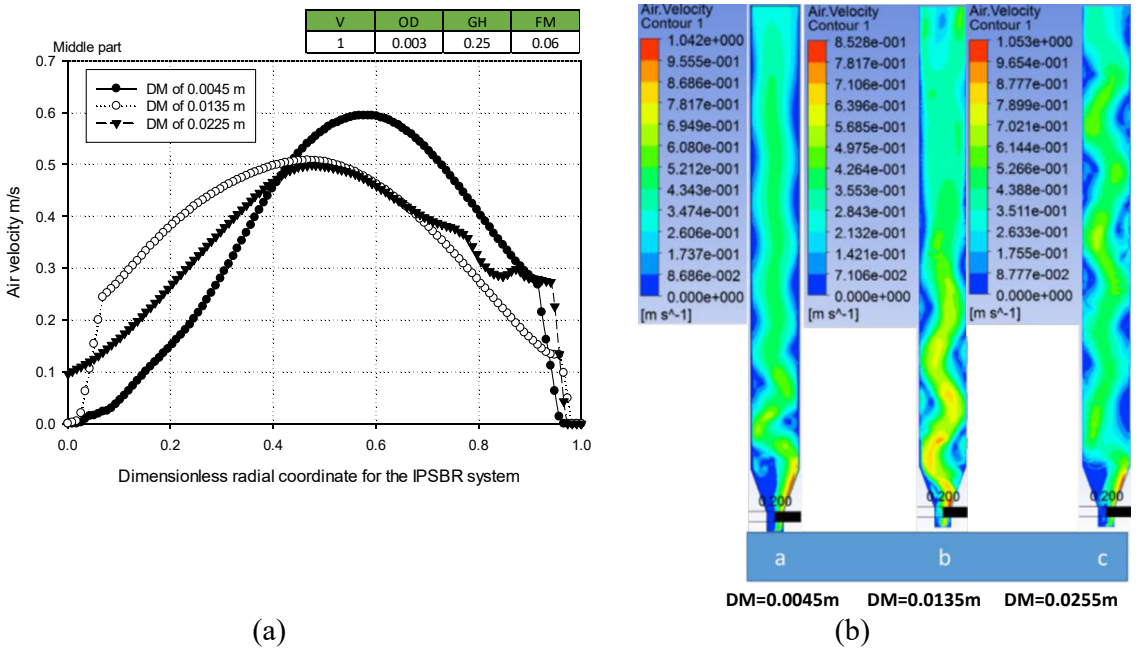


**Figure 7.** (a) Effect of mixing particle diameter on the horizontal profile of the time-averaged air volume fraction at constant feed gas velocity of 1 m/s, orifice diameter of 0.003 m, gas head of 0.25 m and mixing particles loading of 0.06 kg at the middle region, and (b) Eulerian model contours over the three regions for the effect of mixing particle diameter on air velocity distribution at the same fixed conditions.

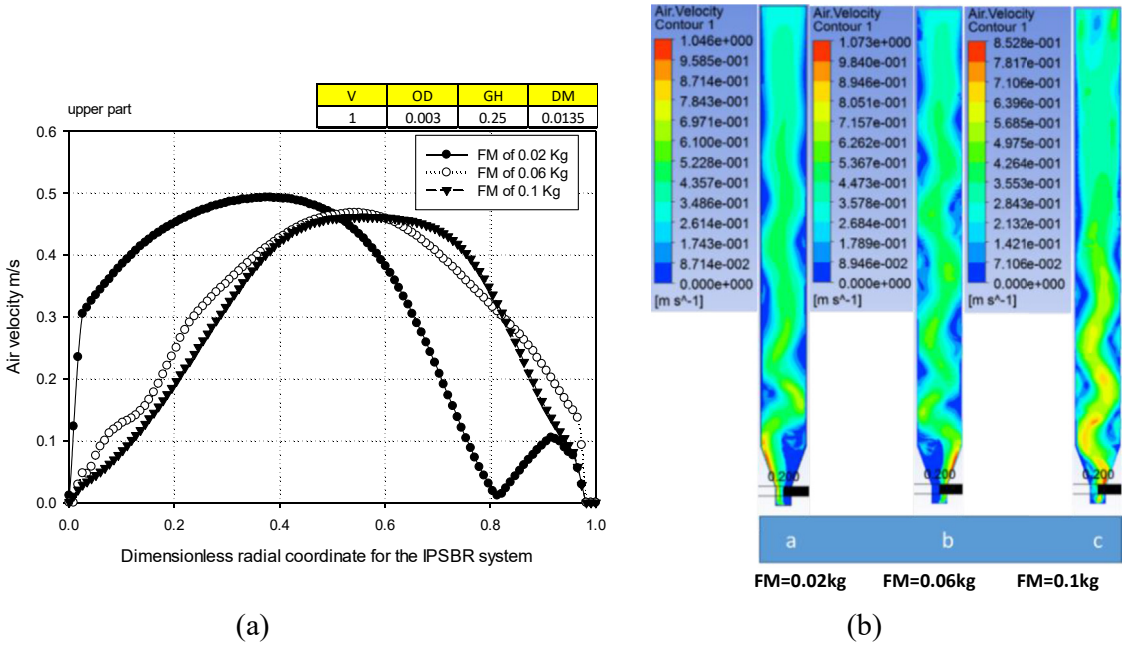


**Figure 8.** (a) Effect of mixing particle loading on the horizontal profile of the time-averaged gas velocity at constant feed gas velocity of 1 m/s, orifice diameter of 0.003 m, gas head of 0.25 m and mixing particles diameter of 0.0135 m at the upper region and (b) Eulerian model contours over the three regions for the effect of mixing particle loading on the air velocity distribution at the same fixed conditions.

velocity profile becomes more uniform and trends toward a parabolic shape, as shown in Figure 6 (a). Near the wall, the air velocity is almost zero because of the no-slip boundary conditions; far from the wall, the air velocity reaches a maximum value at the center of the reactor. From the simulated data of the upper region, it was found that the peak value of air velocity at $x = 0.05$ m is approximately 0.55 m/s for a gas head value of 0.35 m, where $x$ is the dimensionless radial diameter of the system. This result is attributed to the value of the gas head being related to the level of liquid in the column. A smaller gas head means a higher liquid level, which will increase the resistance of air in the column and result in a broad air velocity distribution, thus leading to a higher gas holdup inside the reactor [38]. However, a larger gas head will correspond to a lower liquid level; hence, a narrower air velocity distribution with a higher velocity at the center of the contact system will be observed. This effect is demonstrated in the contours configuration in Figure 6 (b).

d) *Effect of mixing-particle diameter on air velocity distribution*

The influence of the mixing-particle diameter (0.0045, 0.0135, and 0.0225 m) on the air velocity distribution in the middle region at the same constant conditions which were mentioned earlier is demonstrated in Figure 7 (a). Cursory inspection for the simulated data reveals that, at the conical region, the results recorded for the three particle diameters exhibit approximately the same trend. The air velocity is exactly zero near the wall ($x = 0$), increases to a value of almost 1 m/s at $x = 0.06$ m, and then decreases to approximately 0 m/s near the other side wall. By contrast, the air velocity at $x = 0.05$ m and a particle size of 0.0045 m is almost 0.6 m/s and 0.45 m/s in the middle and upper regions, respectively. For particle diameters of 0.0135 and 0.0225 m and at position $x =$ 0.05 m, the air velocity approaches a value of 0.5 and 0.48 m/s in middle and upper regions, respectively.

In summary, the results of the aforementioned analyses show that a decrease in the diameter of the mixing particles to 0.0045 m results in some particles accumulating at the top of the reactor, leading to a concomitant decrease in the recorded air velocity in the upper region. However, the use of larger particles leads to some of the particles settling at the bottom of the reactor and to a decrease in the average air velocity in this region. Particles with an average diameter from 0.0135 to 0.0225 m gave a relatively uniform movement, good mixing within the reactor vessel, and, hence, a lower air velocity. The counter effects are illustrated in Figure 7 (b) and confirm the same findings related to the air velocity distributions for different particle sizes.

e) *Effect of mixing-particle loading on the air velocity distribution*

Figure 8(a) illustrates the air velocity profiles obtained along the contact-system diameter for mixing-particle loading of 0.1, 0.02, and 0.06 kg at the upper region. The effect was examined at a constant feed-gas velocity of 1 m/s, orifice diameter of 0.003 m, gas head of 0.25 m, and mixing-particle diameter of 0.0135 m. From the simulated data, it was found that the air velocity distribution is not uniform in the conical region compared with the distributions in the middle and upper regions, where the distributions are well expressed by the parabolic profile. In the conical region, the disturbance of mixing particles was very high and bubbles were produced in the higher-turbulence region, increasing the overall intensity of the bubbles. The non-uniform distribution of solids is closely related to the flow of gas. As the gas flows through from the bottom to the middle and upper regions, the coalescence and breakup of bubbles begins to decrease because the particles are well distributed. The air velocity also clearly decreases in the middle and upper regions with increasing loading of the mixing particles, which is strongly related to the increase in flow resistance resulting from the increased concentration of the mixing particles over the selected sectional areas. The contours of the of air velocity distribution under different mixing-particle loading is illustrated in Figure 8 (b).

### 4.2. Effect of independent parameters on the air volume fraction

a) *Effect of feed-gas velocity on the air volume fraction*

By comparing the effect of the feed-gas velocity of 1.5 m/s with the effects of velocities of 1 and 0.5 m/s in all of the column regions and under the same constant conditions, it was noted that the maximum air volume fractions along the lateral axis occur at a feed-gas velocity of 1.5 m/s. This result was expected because, in the presence of particles and at a high gas velocity, the air will be better distributed and the water fraction will

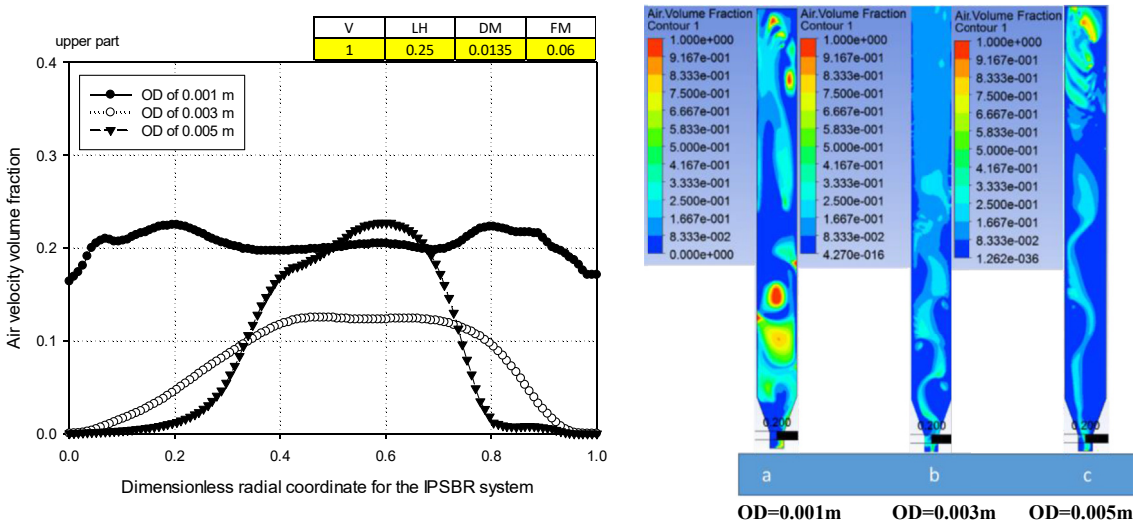


(a) (b)

**Figure 9.** Effect of orifice diameter on the horizontal profile of the time-averaged air volume fraction at constant feed gas velocity of 1 m/s, gas head of 0.25 m, mixing particles diameter of 0.0135 m and mixing particles loading of 0.06 kg at the upper region and (b) Eulerian model contours over the three regions for the effect of orifice diameter on air volume fraction at the same fixed conditions.

decrease since gas volume is increased [39]. In addition, increasing the inlet gas flow rate resulted in an increase in the gas hold-up and accordingly an increase in the gas volume fraction was observed [34].

b) Effect of orifice diameter on air volume fraction

The effect of the orifice diameter was examined under a constant feed-gas velocity of 1 m/s, gas head of 0.25 m, mixing-particle diameter of 0.0135 m, and mixing-particle loading of 0.06 kg. The effect is clearly illustrated by comparing the middle and upper regions with the conical region, where a substantial disturbance in the gas bubbles is observed. It was concluded from Figure 9 (a) that the air bubbles are distributed very well along the reactor diameter in the case of the smallest orifice diameter (0.001 m). Moreover, the maximum value of the volume fraction of air was recorded at the same orifice diameter of 0.001 m. This observation has already been explained, where the superficial velocity and gas holdup increase with decreasing bubble size, resulting in a greater interfacial contact area between the gas and the liquid [34]. The contours corresponding to this study are shown in Figure 9 (b).

c) Effect of gas head on air volume fraction

It was expected that the conical region will not give clear results for the exact effect of the gas head for the reasons previously mentioned. However, the results corresponding to the middle and upper regions reveal that, with increasing gas head, which corresponds to a decrease in water level, the gas

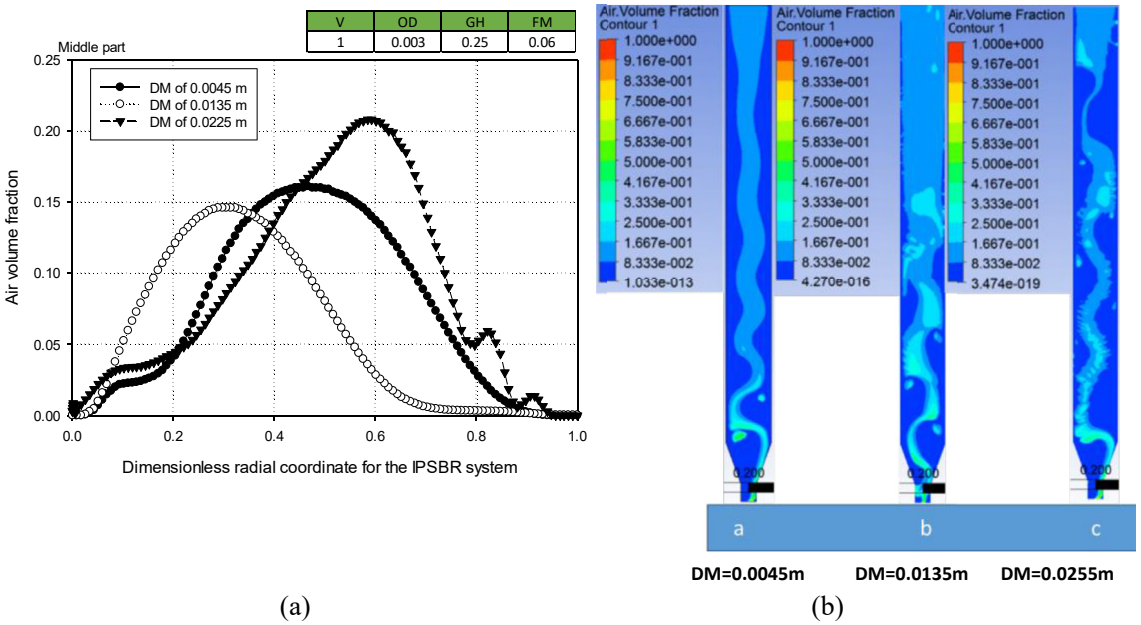


(a) (b)

**Figure 10.** (a) The effect of mixing particle diameter on the horizontal profile of the time-averaged air volume fraction at constant feed gas velocity of 1 m/s, orifice diameter of 0.003 m, gas head of 0.25 m and mixing particles loading of 0.06 kg at the middle region and (b) Eulerian model contours over the three regions for the effect of mixing particle diameter on air volume fraction at same fixed conditions.

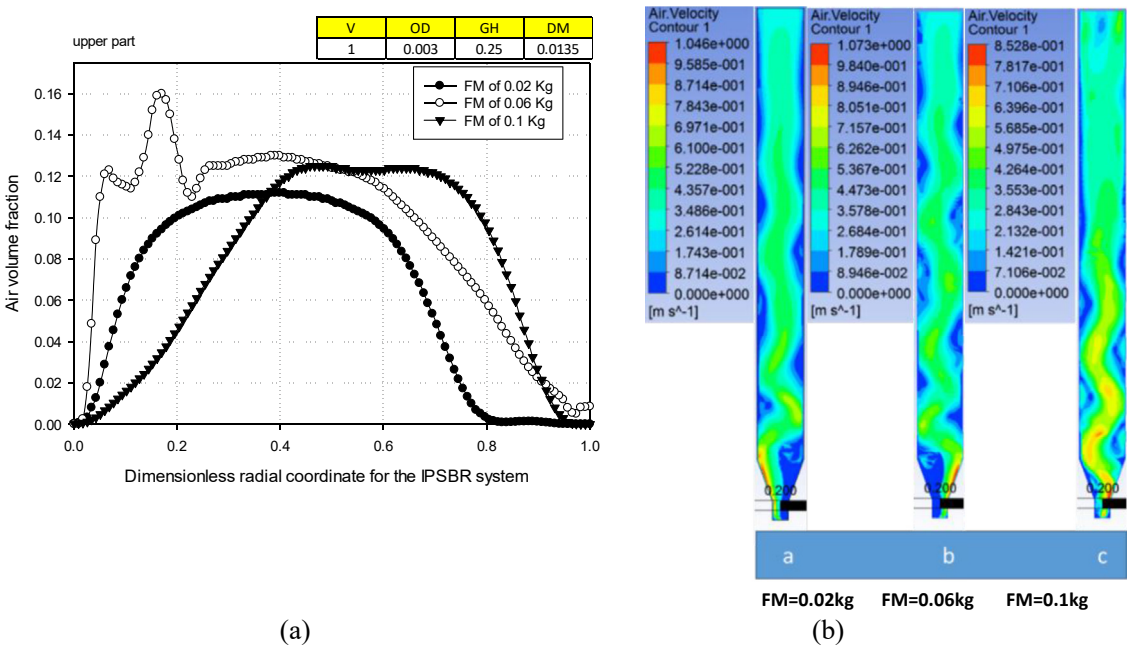


**Figure 11.** (a) Effect of mixing particle loading rate on the horizontal profile of the time-averaged air volume fraction at constant feed gas velocity of 1 m/s, orifice diameter of 0.003 m, gas head of 0.25 m and mixing particles diameter of 0.0135 m at the upper region and (b) Eulerian model contours over the three regions for the effect of mixing particle loading on the air velocity distribution at the same fixed conditions.

volume distribution over the axial dimension is greatly reduced such that most of the gas is concentrated in the center of the contact system and minimal gas is located near the walls. This can be explained by the reduction of liquid head and the corresponding decrease of the flow resistance, which concentrates the gas volume distribution at the center of the contact system as a sharper peak profile [40, 41]. In addition, the gas bubbles, and thus the gas volume fraction, tend to increase toward the walls of the contact system more than at the center in the case of minimum gas head (maximum liquid head), resulting in a broader gas volume profile [42].

d) Effect of mixing-particle diameter on the air volume fraction

The variation in the air volume fraction along the reactor diameter for mixing-particle diameters of 0.0045, 0.0135, and 0.0225 m at the conical, middle, and upper regions was studied. The variation in the air volume fraction was examined at a constant feed-gas velocity of 1 m/s, orifice diameter of 0.003 m, gas head of 0.25 m, and mixing-particle loading of 0.06 kg. The bubble dispersion is more evident in the middle region. Figure 10 (a) indicates that, with the injection of 0.0225 m diameter particles, the gas bubbles are well dispersed at the wall as well as at the center. As the diameter decreases, the distribution at the wall and center decreases because of a decrease in intensity of the circulation and eddies inside the contact system. By contrast, in the upper region, the gas was found to be more distributed at the wall when 0.0045 or 0.0135 m particles are used than when 0.00225 m particles are used. This was expected because these particles have a lower mass and thus accumulate at the upper part of the reactor, leading to greater dispersion of the bubbles at the wall. The contours extracted for this investigation are shown in Figure 10 (b).

e) Effect of mixing-particle loading on air volume fraction

Figure 11 (a) shows an overview of the change in air volume fraction with respect to the mixing-particle loading at a constant feed-gas velocity of 1 m/s, orifice diameter of 0.003 m, gas head of 0.25 m, and mixing-particle diameter of 0.0135 m at the upper region. Notably, as the particle loading increase, the air volume fraction increases, where bubbles will be broken, especially in the conical region. In addition, the liquid velocity is expected to increase, which will result in higher gas holdup. Moreover, the collisions between the liquid and gas will increase, resulting in an increase in the interfacial area and accordingly a higher air volume fraction. Figure 11 (b) shows the air volume fraction contours along the reactor diameter.

### 4.3. Influences of factors on air velocity

The simulated results for air velocity obtained under various operating parameters designed under the RSM are shown for the three examined regions in Tables S1, S2, and S3, respectively (See supplementary content). According to these responses, a second-order polynomial response equation in terms of dependent (air velocity) and significant independent coded variables (velocity (m/s), orifice diameter (m), gas head over liquid (m), diameter of mixing particles (m), mixing particles loading (kg) and their interactions) for the conical, middle, and upper regions are given by Eqs. (11), (12), and (13), respectively:

Time-averaged conical air velocity (m/s)

$$= -0.8745 + 0.2008\,x_1 + 174.0\,x_2 + 3.301\,x_3 + 27.03\,x_4 + 5.502 - x_5 0.1308\,x_1^2 - 23701\,x_2^2 - 5.691\,x_3^2 - 382.1\,x_4^2 - 35.36\,x_5^2 + 52.13\,x_1x_2 - 66.7\,x_2x_3 - 198.1\,x_2x_5 - 29.74\,x_3x_4 + 4.05\,x_3x_5 - 93.9\,x_4x_5 \quad (13)$$

Time-averaged middle air velocity (m/s)

$$= -0.5012 - 0.0977x_1 + 120.23x_2 + 2.362x_3 + 21.73x_4 + 5.892x_5 - 0.0747x_1^2 - 12908x_2^2 - 3.756x_3^2 - 301.4x_4^2 - 21.38x_5^2 + 0.5561x_1x_3 + 1.555x_1x_5 - 22.37x_3x_4 - 15.87 - 81.9x_4x_5 \quad (14)$$

Time-averaged upper air velocity (m/s)

$$= 0.6581 + 38.07\,x_2 - 22.24\,x_4 - 0.0397\,x_1^2 - 7642\,x_2^2 + 4.122\,x_3^2 + 320.7\,x_4^2 + 9.33\,x_5^2 - 0.4880x_1x_3 + 5.523\,x_1x_4 + 3.442\,x_1x_5 + 146.1\,x_2x_3 + 1988\,x_2x_4 - 4.61\,x_3x_5 + 53.7\,x_4x_5 \quad (15)$$

where $x_1$, $x_2$, $x_3$, $x_4$, and $x_5$ are coded variables.

The results of the RSM fitting in the form of analysis of variance (ANOVA) are shown in Tables S4, S5, and S6 for the conical, middle, and upper regions, respectively. The adequacy of the second-order response surface model was checked by Fisher's *F*-test, its associated probability $P(F)$, and its $R^2$ value, which indicates how well the regression model fits the trend of the results. Results obtained with the model are significant if their *p*-value is less than 0.05. Results with *p*-values greater than 0.05 are considered statistically insignificant at the 95% confidence level [43, 44].

For the conical region, the high $R^2$ value of 99.78% and small standard deviation value of 0.00443 indicate that the full quadratic model best fits the obtained results. The results corresponding to the model are significant if $p < 0.05$. As demonstrated in Table S4, most of the results are significant, except for the interaction between velocity and gas head, velocity and diameter of mixing particles, and velocity and mixing particles loading, where the *p*-values are greater than 0.05.

Table S5 shows the results obtained from the regression model for air velocity in the middle region; this model was selected because of the high corresponding $R^2$ (99.87%) and small standard deviation (0.00443) values. According to the *p*-values, all of the independent parameters had a significant effect on the air velocity. However, the interaction effects between the velocity and orifice diameter, velocity and particle diameter, orifice diameter and gas head, orifice and particle dimeter, and the orifice diameter and mixing particles loading are all insignificant because the corresponding *p*-values are greater than 0.05.

Similar to the results for the conical and middle regions, those for the upper region were well fit by the regression equation, as indicated by the high $R^2$ and small standard deviation values, as illustrated in Table S6. However, the *p*-values for the velocity, gas head, and mixing-particle loading are 0.337, 0.056, and 0.247, respectively, implying that these variables are not significant. In addition, the interaction between the velocity and orifice diameter, orifice diameter and mixing-particle loading, and gas head and particle diameter are also minor, as indicated by the high corresponding *p*-values reported in Table S6.

Residual analysis is another tool to understand how the model fits the trend of the obtained results. A residual is the difference between an observed value and its corresponding fitted value.

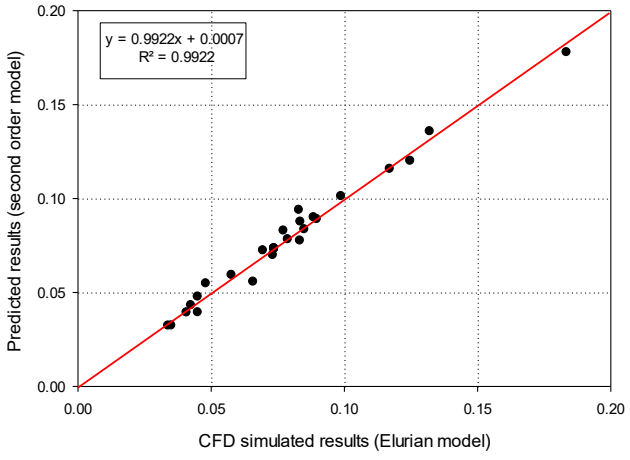


**Figure 12.** The relationship between CFD simulated results (Eulerian model) and predicted results (second order model) for the same response at the same conditions.

Residual plots were used to assess the quality of the regression fit for the air velocity response in the conical, middle, and upper regions [45]. The results indicated that the model is adequate and in a good agreement with the simulated data.

### 4.4. Influences of factors on air volume fraction

From the CCD regression analysis, the full quadratic models representing the air volume fraction are expressed by Eqs. (14), (15), and (16) for the conical, middle, and upper regions of the reactor, respectively:

Time-averaged conical air volume fraction

$$= 0.0499 + 0.0060\,x_1 + 26.85\,x_2 - 0.374\,x_5 + 0.05999\,x_1^2 + 9040\,x_2^2 + 0.423\,x_3^2 - 59.65\,x_1x_2 - 0.2767\,x_1x_3 + 5.670\,x_1x_4 + 1.1201\,x_1x_5 + 37.38\,x_2x_3 - 958.7\,x_2x_4 - 252.2\,x_2x_5 + 3.92\,x_3x_4 + 20.98\,x_4x_5 \quad (16)$$

Time-averaged middle air volume fraction

$$= 0.0837 + 0.2947\,x_1 - 70.26\,x_2 + 0.030\,x_3 + 0.72\,x_4 - 2.202x_5 + 0.08745\,x_1^2 + 12502\,x_2^2 + 1.050\,x_3^2 + 267.4\,x_4^2 - 63.86\,x_1x_2 - 0.8504\,x_1x_3 + 2.762\,x_1x_4 + 203.3\,x_2x_3 - 1670\,x_2x_4 - 42.81\,x_3x_4 + 1.914\,x_3x_5 + 96.04\,x_4x_5 \quad (17)$$

Time-averaged upper air volume fraction

$$= -0.3421 + 0.4960\,x_1 + 7.7\,x_2 + 0.985\,x_3 + 4.29\,x_4 + 0.377\,x_5 + 18788\,x_2^2 - 34.74\,x_1x_2 - 0.854\,x_1x_3 - 1.104\,x_1x_5 - 3893\,x_2x_4 - 1003.1\,x_2x_5 + 4.84\,x_3x_5 + 173.2\,x_4x_5 \quad (18)$$

where $x_1$, $x_2$, $x_3$, $x_4$, and $x_5$ are coded variables.

The computational results were analyzed using ANOVA to detect the most significant parameter with respect to the air volume fraction. The *F*-values (*F*), *p*-values, and $R^2$ values for the influence of different parameters on the response in the conical, middle, and upper regions were determined. The results show that the $R^2$ values in all of the regions approach unity and that the standard deviation value is very low, indicating better prediction of response and a good fit of the model to the computed data [46]. ANOVA analysis for time-averaged conical air velocity showed that the linear coefficients and quadratic coefficients of gas head and particle diameter were found to be not significant according to the *p*-values, which are greater than 0.05. The cross-product coefficient (gas head and mixing-particle loading) is also unimportant, with a *p*-value of 0.236. In contrast, ANOVA analysis for time-averaged middle air volume fraction reveals that all of the independent parameters have significant effects, with *p*-values less than 0.05. However, the two-way interactions between the velocity and the mixing-particle loading and between the orifice diameter and the mixing-particle loading are not significant ($p > 0.05$). In the case of the upper region, all of the linear coefficients are positive. However, none of the quadratic coefficients are significant except for the quadratic interaction of the orifice diameter, which has a *p*-value less than 0.05. In addition, the two-way interactions between the velocity and particle diameter, the orifice diameter and gas head, and the gas head and mixing diameter are minor in this region.

The adequacy of the results was confirmed by residual plots for the three regions [35]. The transformed data in the normal probability plot were found to be very close to the normality distribution curve. In other words, the results obtained from the simulated Eulerian model is very close to the statistical results obtained from the second order regression. Moreover, residuals versus order plot fluctuates, showed that there is no pattern and therefore indicating independency. Figure 12 provide further confirmation of the acceptability of the model. All of the collected data show a good distribution of CFD simulated data and predicted values, as no difference is observed among them.

**Table 2.** Optimum condition and fitted responses with composite desirability of one.

| Solution | V (m) | OD (m) | GH (m) | DM (m) | FM (kg) |
|---|---|---|---|---|---|
| | 1.5 | 0.001 | 0.164141 | 0.0225 | 0.02 |
| $R_1$ Fit | $R_2$ Fit | $R_3$ Fit | $R_4$ Fit | $R_5$ Fit | $R_6$ Fit | Composite Desirability |
| 0.306612 | 0.482094 | 0.178463 | 0.124708 | 0.046156 | 0.0065811 | **1** |

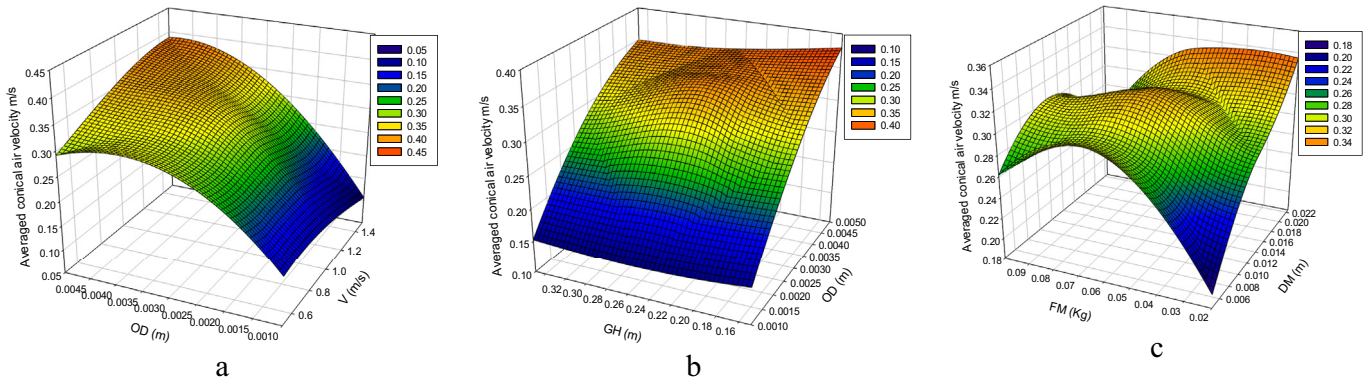


**Figure 13.** Time-averaged conical air velocity on 3-D graphics for response surface optimization versus (a) feed gas velocity and orifice diameter, (b) orifice diameter and gas head, (c) mixing particles diameter and mixing particles loading

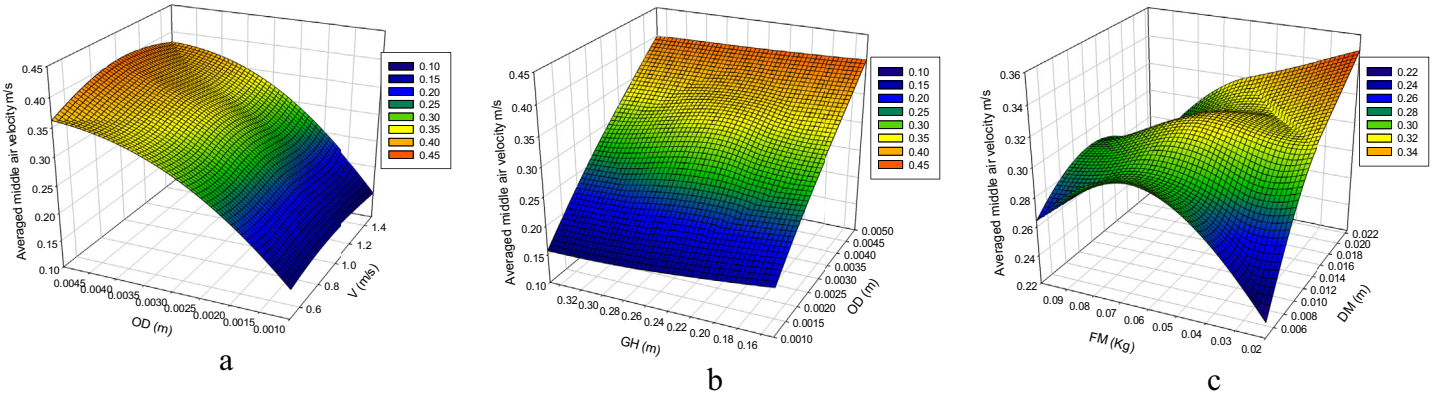


**Figure 14.** Time-averaged middle air velocity on 3-D graphics for response surface optimization versus (a) feed gas velocity and orifice diameter, (b) orifice diameter and gas head, (c) mixing particles diameter and mixing particles loading.

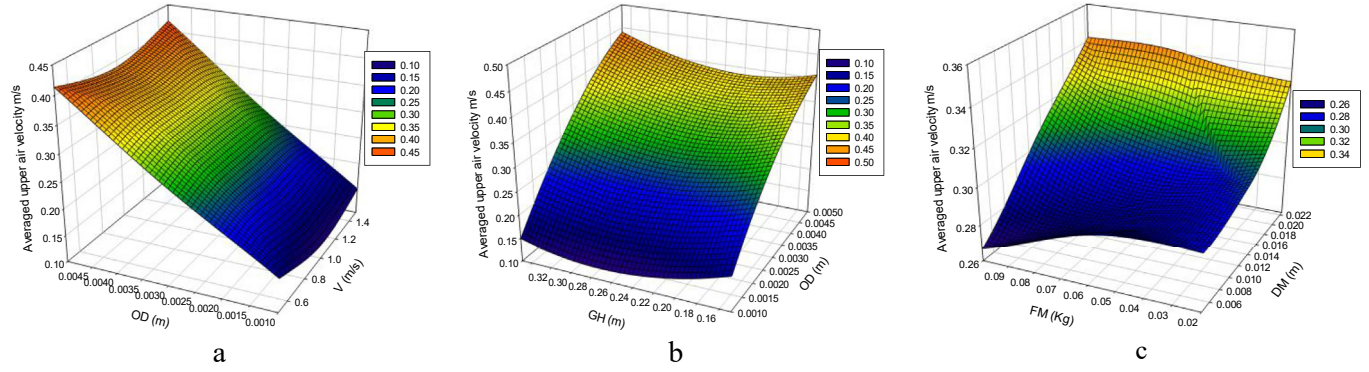


**Figure 15.** Time-averaged upper air velocity on 3-D graphics for response surface optimization versus (a) feed gas velocity and orifice diameter, (b) orifice diameter and gas head, (c) mixing particles diameter and mixing particles loading.

### 4.5. Response optimizer

The regression model was used to determine the optimum operating parameters obtained using the response optimizer in Minitab, as listed in Table 2. It represents the extent to which the corresponding setting optimizes various response parameters in general [47]. The desirable upper, middle and conical air volume fractions ($R_1$, $R_2$ and $R_3$, respectively) were targeted to be maximum to achieve maximum interfacial area concentration, whereas the desirable upper, middle and conical air velocities ($R_4$, $R_5$ and $R_6$, respectively) were targeted to be minimal to achieve maximum gas residence time. The prediction of the optimizer shows that the lowest average air velocity and highest average air volume fraction in the conical, middle, and upper regions were achieved with parameters of a feed-gas velocity of 1.5 m/s, orifice diameter of 0.001 m, gas head of 0.164 m, mixing-particle diameter of 0.0225 m, and mixing-particle loading of 0.02 kg. Notably, the optimum responses were reached at the highest feed-gas velocity of 1.5 m/s. This result reflects that the IPSBR can operate at a high feed-gas velocity while maintaining a high gas residence time and a high gas volume fraction. It also makes the contact system more economical with respect to operating costs and operating time.

### 4.6. Three-dimensional surface plots

A three-dimensional (3-D) graph can also be used to represent the RSM results [13]. As an example, Figures 13, 14, and 15 show the effect of some interactions (feed gas velocity-orifice diameter, orifice diameter-gas head, and mixing particle diameter-mixing particles loading) on the average air velocity in the three different regions of the contact system. The curvature of the surface plots indicates the presence of significant nonlinear relationships between the parameters. The interactions between the factors are also demonstrated in these figures, which reveal the same results discussed in Section 4.2.

3D drawings have been plotted for the two responses (air velocity distribution and volume fraction) versus all possible factor's interaction show that the minimum average air velocity and maximum average air volume fraction can be achieved at a high feed-gas velocity, low orifice diameter, gas head, and mixing-particle loading, and intermediate particle diameter, which supports the previously discussed results. Operating the reactor under optimized parameters that give a high air volume fraction is important for ensuring a large gas–liquid contact area and, hence, a higher interfacial area concentration and mass transfer coefficient. Furthermore, the minimum average air velocity will increase the gas residence time, which will enhance the gas reactivity in the liquid phase. A suitable particle diameter is very important for the distribution of particles within the contact system because heavy particles are expected to settle, whereas low-weight particles will accumulate at the top of the reactor. In addition, as mentioned in sections 4.1 and 4.2, a small orifice diameter is preferred because it will produce small gas bubbles with high surface areas, which in turn increases the gas holdup and residence time. Moreover, a minimum gas head is preferred because it is accompanied by an increase in the liquid level, providing greater resistance for the gas flow. A wide gas volume fraction profile and maximum average gas volume fraction are also observed. Under these conditions, the contact system is expected to be more economical to operate and the overall performance of the reactor should be enhanced.

## 5. Conclusions

In this work, the effects of operating conditions (i.e., feed-gas velocity, orifice diameter, gas head, mixing-particle diameter, and mixing-particle loading) were analyzed using CFD simulations for the IPSBR system. A full-factorial CCD was used to analyze the relationship between the aforementioned operating conditions and the average air velocity and air volume fraction in three sectional areas of the contact system (i.e., the conical, middle, and upper regions). The optimum responses using average data can be attained under conditions at a feed-gas velocity of 1.5 m/s, orifice diameter of 0.001 m, gas head of 0.164 m, mixing-particle diameter of 0.0225 m, and mixing-particle loading of 0.02 kg, with confidence level of 95%.

The unique effect of the inner mixing particles on the performance of the contact system will be studied in more comprehensive future work, where the effect of the operating conditions on the inner particles' average velocity, the average volume fraction, the particle mass concentration, and the eddy viscosities will be analyzed and optimized to ensure a uniform distribution of inert particles over the three contact-system regions.

## Declarations

### Author contribution statement

A. Mohammad & A. A-H. I. Mourad: Performed the experiments; Analyzed and interpreted the data; Wrote the paper.

M. H. El-Naas: Conceived and designed the experiments; Analyzed and interpreted the data.

B. Van der Bruggen & F. Alnaimat: Conceived and designed the experiments.

A. H. Al-Marzouqi: Conceived and designed the experiments; Wrote the paper.

M. Al-Marzouqi, M. Suleiman & M. Al Musharfy: Contributed reagents, materials, analysis tools or data.

### Funding statement

This work was supported by the ADNOC Refining Research Center, Abu Dhabi, UAE.

### Data availability statement

Data will be made available on request.

### Declaration of interests statement

The authors declare no conflict of interest.

### Additional information

Supplementary content related to this article has been published online at https://doi.org/10.1016/j.heliyon.2021.e06369.

## Acknowledgements

The authors would also like to thank Dr. Tommy Firmansyah from ADNOC Refining Research Center, Jawad Mustafa from Chemical Engineering Department, Abeer Fuad from Architectural Engineering Department, Amin Safi, and Zahid Qureshi from Mechanical Engineering at the UAE University for their assistance.

## References

[1] M.H. El-Naas, A.F. Mohammad, M.I. Suleiman, M. Al Musharfy, A.H. Al-Marzouqi, Evaluation of a novel gas-liquid contactor/reactor system for natural gas applications, J. Nat. Gas Sci. Eng. 39 (2017) 133–142.

[2] M.H. El-Naas, System for Contacting Gases and Liquids, 8 , Aug. 2017. U.S. Patent No. 9,724,639.

[3] J. Mustafa, A.H.I. Mourad, A.H. Al-Marzouqi, M.H. El-Naas, Simultaneous treatment of reject brine and capture of carbon dioxide: a comprehensive review, Desalination 483 (2020) 114386.

[4] M.H. Ibrahim, M.H. El-Naas, R. Zevenhoven, S.A. Al-Sobhi, Enhanced CO2 capture through reaction with steel-making dust in high salinity water, Int. J. Greenh. Gas Control 91 (2019/12/01/2019) 102819.

[5] A.F. Mohammad, A.H.I. Mourad, J. Mustafa, A.H. Al-Marzouqi, M.H. El-Naas, M.H. Al-Marzouqi, F. Alnaimat, M. Suleiman, M. Al Musharfy, T. Firmansyah,

Computational fluid dynamics simulation of an inert particles spouted bed reactor (IPSBR) system, Int. J. Chem. React. Eng. 18 (5–6) (2020), 20200025.
[6] X.L. Zhao, S.Q. Li, G.Q. Liu, Q. Yao, J.S. Marshall, DEM simulation of the particle dynamics in two-dimensional spouted beds, Powder Technol. 184 (2) (2008) 205–213.
[7] X. Jiang, W. Zhong, X. Liu, B. Jin, Study on gas-solid flow behaviors in a spouted bed at elevated pressure: numerical simulation aspect, Powder Technol. 264 (2014) 22–30.
[8] B. Ren, W. Zhong, B. Jin, Z. Yuan, Y. Lu, Computational fluid dynamics (CFD)–discrete element method (DEM) simulation of gas–solid turbulent flow in a cylindrical spouted bed with a conical base, Energy Fuels 25 (9) (2011) 4095–4105.
[9] B. Ren, Y. Shao, W. Zhong, B. Jin, Z. Yuan, Y. Lu, Investigation of mixing behaviors in a spouted bed with different density particles using discrete element method, Powder Technol. 222 (2012) 85–94.
[10] S.H. Hosseini, G. Ahmadi, M.R. Rahimi, M. Kiani, Study of pressure drop in the 2D spouted bed with conical base of binary particle mixtures: effects of particle size and density, Iran. J. Chem. Chem. Eng. (Int. Engl. Ed.) 37 (2) (2018) 183–192.
[11] M. Dutka, M. Ditaranto, T. Løvås, Application of a central composite design for the study of NOx emission performance of a low NOx burner, Energies 8 (5) (2015) 3606–3627.
[12] K.G. Santos, M.C.C. Francisquetti, R.A. Malagoni, M.A.S. Barrozo, Fluid dynamic behavior in a spouted bed with binary mixtures differing in size, Dry. Technol. 33 (14) (2015) 1746–1757.
[13] H. Pashaei, A. Ghaemi, M. Nasiri, B. Karami, Experimental modeling and optimization of CO2 absorption into piperazine solutions using RSM-CCD methodology, ACS Omega 5 (15) (2020) 8432–8448.
[14] A. Nuchitprasittichai, S. Cremaschi, Optimization of CO2 capture process with aqueous amines using response surface methodology, Comput. Chem. Eng. 35 (8) (8/10/2011) 1521–1531.
[15] M. Gholamzadehdevin, L. Pakzad, Hydrodynamic characteristics of an activated sludge bubble column through computational fluid dynamics (CFD) and response surface methodology (RSM), Can. J. Chem. Eng. 97 (4) (2019) 967–982.
[16] L.-Y. Liang, Y.-G. Zheng, Y.-C. Shen, Optimization of β-alanine production from β-aminopropionitrile by resting cells of Rhodococcus sp. G20 in a bubble column reactor using response surface methodology, Process Biochem. 43 (7) (2008) 758–764.
[17] M. Aghbolaghy, A. Karimi, Simulation and optimization of enzymatic hydrogen peroxide production in a continuous stirred tank reactor using CFD–RSM combined method, J. Taiwan Inst. Chem. Eng. 45 (1) (2014) 101–107.
[18] M.V. Prabhu, R. Karthikeyan, Comparative studies on modelling and optimization of hydrodynamic parameters on inverse fluidized bed reactor using ANN-GA and RSM, Alexandria Eng. J. 57 (4) (2018) 3019–3032.
[19] N. Masmoudi, Incompressible, Inviscid Limit of the Compressible Navier-Stokes System second ed., vol. 18, 2001, pp. 199–224.
[20] J. Sanyal, S. Vásquez, S. Roy, M.P. Dudukovic, Numerical simulation of gas–liquid dynamics in cylindrical bubble column reactors, Chem. Eng. Sci. 54 (21) (1999) 5071–5083.
[21] F. Marchelli, C. Moliner, B. Bosio, E. Arato, A CFD-DEM sensitivity analysis: the case of a pseudo-2D spouted bed, Powder Technol. 353 (2019) 409–425.
[22] Z. Zhang, C. Yang, Y. Zhang, H. Zhu, Dynamic modeling method for infrared smoke based on enhanced discrete phase model, Infrared Phys. Technol. 89 (2018) 315–324.
[23] S.A.J. Morsi, A.J. Alexander, An investigation of particle trajectories in two-phase flow systems, J. Fluid Mech. 55 (2) (1972) 193–208.
[24] S.V. Patankar, Numerical Heat Transfer and Two-phase Yow, Hemisphere, Washington DC, 1980.
[25] A. Kartushinsky, S. Tisler, J.L.G. Oliveira, C.W.M. van der Geld, Eulerian-Eulerian modelling of particle-laden two-phase flow, Powder Technol. 301 (2016/11/01) 999–1007.
[26] G. Li, X. Yang, G. Dai, CFD simulation of effects of the configuration of gas distributors on gas–liquid flow and mixing in a bubble column, Chem. Eng. Sci. 64 (24) (12/16/2009) 5104–5116.
[27] Z. Li, X. Guan, L. Wang, Y. Cheng, X. Li, Experimental and numerical investigations of scale-up effects on the hydrodynamics of slurry bubble columns, Chin. J. Chem. Eng. 24 (8) (2016/08/01/2016) 963–971.
[28] R.H. Myers, D.C. Montgomery, C.M. Anderson-Cook, Process and product optimization using designed experiments, Response Surface Methodol. 2 (2002) 328–335.
[29] T. Ölmez, The optimization of Cr (VI) reduction and removal by electrocoagulation using response surface methodology, J. Hazard Mater. 162 (2-3) (2009) 1371–1378.
[30] B.K. Körbahti, M.A. Rauf, Application of response surface analysis to the photolytic degradation of Basic Red 2 dye, Chem. Eng. J. 138 (1-3) (2008) 166–171.
[31] K.-Y. Kim, J.-W. Seo, Shape optimization of a mixing vane in subchannel of nuclear reactor, J. Nucl. Sci. Technol. 41 (5) (2004) 641–644.
[32] J. Antony, Design of Experiments for Engineers and Scientists, Elsevier, 2014.
[33] D. Chakraborty, M. Guha, P.K. Banerjee, CFD simulation on influence of superficial gas velocity, column size, sparger arrangement, and taper angle on hydrodynamics of the column flotation cell, Chem. Eng. Commun. 196 (9) (2009) 1102–1116.
[34] B. Moshtari, E.G. Babakhani, J.S. Moghaddas, Experimental study of gas hold-up and bubble behavior in gas-liquid bubble column, Petroleum Coal 51 (1) (2009) 27–32.
[35] M. Bouaifi, G. Hebrard, D. Bastoul, M. Roustan, A comparative study of gas hold-up, bubble size, interfacial area and mass transfer coefficients in stirred gas–liquid reactors and bubble columns, Chem. Eng. Process: Process Intensification 40 (2) (2001) 97–111.
[36] H. Luo, H.F. Svendsen, Theoretical model for drop and bubble breakup in turbulent dispersions, AIChE J. 42 (5) (1996) 1225–1233.
[37] M.J. Prince, H.W. Blanch, Bubble coalescence and break-up in air-sparged bubble columns, AIChE J. 36 (10) (1990) 1485–1499.
[38] A. Behkish, R. Lemoine, L. Sehabiague, R. Oukaci, B.I. Morsi, Gas holdup and bubble size behavior in a large-scale slurry bubble column reactor operating with an organic liquid under elevated pressures and temperatures, Chem. Eng. J. 128 (2) (2007/04/01) 69–84.
[39] D.N. Smith, W. Fuchs, R.J. Lynn, D.H. Smith, M. Hess, Bubble Behavior in a Slurry Bubble Column Reactor Model, ACS Publications, 1984.
[40] E. Delnoij, J.A.M. Kuipers, W.P.M. van Swaaij, A three-dimensional CFD model for gas–liquid bubble columns, Chem. Eng. Sci. 54 (13-14) (1999) 2217–2226.
[41] G.L. Lane, M.P. Schwarz, G.M. Evans, Modelling of the Interaction between Gas and Liquid in Stirred Vessels, Elsevier, 2000, pp. 197–204.
[42] N.P. Cheremisinoff, P.N. Cheremisinoff, Hydrodynamics of Gas-Solids Fluidization, 1984.
[43] Y.-L. Gao, X.-R. Ju, Statistical prediction of effects of food composition on reduction of Bacillus subtilis as 1.1731 spores suspended in food matrices treated with high pressure, J. Food Eng. 82 (1) (2007) 68–76.
[44] H. Zhao, H.-R. Hu, Optimal design of a pipe isolation plugging tool using a computational fluid dynamics simulation with response surface methodology and a modified genetic algorithm, Adv. Mech. Eng. 9 (10) (2017), 1687814017715563.
[45] D.C. Montgomery, Design and Analysis of Experiments, John wiley & sons, 2017.
[46] A.A. Guinta, Aircraft Multidisciplinary Design Optimization Using Design of Experimental Theory and Response Surface Modeling Methods, Ph. D. Thesis., Department of Aerospace Engineering, 1997.
[47] A.A.-H.I. Mourad, N.M. Ghasem, A.Y. Alraeesi, Modelling and simulation of hydrogen production via water gas shift membrane reactor, Int. J. Chem. Eng. Appl. 9 (4) (2018).